ARTICLE

OPEN

Check for updates

Simultaneous effect of strain rate and humidity on the structure and mechanical behavior of spider silk

Kenjiro Yazawa[1], Ali D. Malay [1], Hiroyasu Masunaga[2,3], Y. Norma-Rashid [4] & Keiji Numata [1✉]

Spider dragline silk fibers are important in nature for capturing prey and as a lifeline. However, spider silk is exposed to a range of humidity and deformation conditions, and it is important to understand what effect these have on its properties. Here, we simultaneously investigated the effect of a wide range of strain rates on the structural and mechanical properties of spider silk under different humidity conditions. The toughness of the silk fiber was enhanced under mild humidity and high deformation rate conditions, which occur in the natural habitat of spiders. Structural changes in the fiber upon tension were monitored with a wide-angle X-ray scattering system, showing that during stretching the orientation of the crystalline β-sheets aligned, whereas the crystallite size decreased. These findings help to understand the link between the structural changes and mechanical behavior of spider silk.

[1] Biomacromolecules Research Team, RIKEN Center for Sustainable Resource Science, 2-1 Hirosawa, Wako-shi, Saitama 351-0198, Japan. [2] Japan Synchrotron Radiation Research Institute, 1-1-1, Kouto, Sayo-cho, Sayo-gun, Hyogo 679-5198, Japan. [3] Research Infrastructure Group, RIKEN SPring-8 Center, 1-1-1, Kouto, Sayo-cho, Sayo-gun, Hyogo 679-5148, Japan. [4] Institute of Biological Science, Faculty of Science, University of Malaya, Kuala Lumpur 50603, Malaysia. ✉email: keiji.numata@riken.jp

Spider dragline silk is a unique biomaterial noted for its excellent toughness, ductility, and strength[1,2]. Dragline silk fiber is used as a major component in web construction, and thus critical for prey capture, and also functions as a lifeline for the spider[3]. In the natural state, the dragline fibers need to function under a wide range of conditions; for instance, relative humidity (RH) varies depending on the environmental conditions, which can have a considerable effect on performance[4,5]. Difference in food uptake of spiders depending on their habitats is also known to affect the level of protein expression in the major ampullate silk gland[6]. In addition, the mechanical forces imparted on web silk components would necessarily be different for prey insects flying at various speeds[3]. It is known that the mechanical properties of predominantly amorphous polymeric materials exhibit strain rate sensitivity[7]. At the mesoscale, dragline silk fibers consist of crystalline β-sheets embedded in amorphous regions consisting of α-helices, β-turns, 3_{10}-helices, and random structures; hence, it is possible that the deformation rate can affect the mechanical responses of spider dragline silk.

To date, the effect of strain rate on the mechanical properties of dragline silk fibers has been investigated by several groups[3,8–10]. Denny characterized the dragline silk derived from *Araneus sericatus* and found that the toughness of the silk increased threefold when the strain rate varied from 0.0005 to 0.024 s^{−1}, with concomitant increase in tensile strength and Young's modulus, under RH conditions of 48–52%[9]. In contrast, Cunniff et al. analyzed the dragline silk derived from *Nephila clavipes* and found that increasing the strain rate from 0.1 to 3000 s^{−1} did not influence the toughness, Young's modulus, or elongation at break, at constant RH50%[8]. On the other hand, Gosline et al., using dragline silk from *Araneus diadematus*, found that the toughness increased 10-fold upon varying the strain rate from 0.0005 to 30 s^{−1}; however, they provided no description about the experimental RH conditions[3]. More recently, Hudspeth et al. studied the dragline silk of *Nephila clavipes* and reported that the toughness increased threefold by varying the strain rate from 0.001 to 1700 s^{−1} at RH34%[10]. Thus, although previous investigations have been reported on the effects of strain rate on mechanical properties of spider dragline silk, the effect of varying RH conditions has not been treated systematically. We should consider the effect of humidity to discuss the strain rate-dependent mechanical parameters because the physical properties of spider dragline silk fibers are sensitive to hydration effects[5,11–19].

It is also important to understand the structural change upon deformation because the orientation, size, and fraction of crystalline β-sheets play crucial roles in regulating the strength, stiffness, and toughness of dragline silk fibers[5,20–22]. The structural changes in spider dragline silk fibers during extension have been investigated by several groups[20,22–24]. Sirichaisit et al. detected the structural changes in spider dragline silk fibers during ~25% extension deformation via Raman spectroscopy analysis of single filaments[23,24]. Glišović et al. monitored the strain-dependent structural changes in spider dragline silk using a single-fiber X-ray scattering technique with a microfocus synchrotron beam[20]. In this study, they succeeded in single-fiber wide-angle X-ray scattering (WAXS) measurement of dragline silks under extension, wherein the measurement was based on the alternating stretching and beam radiation, which enabled the relaxation process of the silk molecules during beam radiation. Alternatively, we have previously demonstrated the feasibility of conducting simultaneous tensile deformation studies with synchrotron X-ray beam irradiation on dragline silk bundles derived from *Nephila clavata*[22]. Although such efforts to elucidate the structural changes that occur during the extension of spider dragline silk fibers have been conducted, the effect of humidity on the structural changes in spider dragline silk fibers under extension deformation is still largely unknown. In the present study, we perform simultaneous WAXS and tensile tests under different strain rates and RH conditions to clarify the relationships between deformation rate and humidity on the mechanical and nanoscale structural properties of spider dragline silk fibers.

Results and Discussion

Tensile tests under different strain rates. Tensile tests of dragline silk fibers were conducted at RH43% under different strain rates from 3.3×10^{-5} to 3.3 s^{−1}. The resultant stress–strain curves are shown in Fig. 1. The tensile strength and elongation at break were dependent on the strain rates. The tensile strength and elongation at break increased linearly with increasing strain rate. The mechanical properties of the dragline silk fiber at RH43% under different strain rates are displayed in Fig. 2. The tensile strength and elongation at break exhibited a 1.7-fold and 1.6-fold increase as the strain rate increased from 3.3×10^{-5} to 3.3 s^{−1}, respectively. The increase in tensile strength could be attributed to the more crystalline β-sheet orientation at the higher strain rate, contributing to higher Young's modulus[10]. The increase in elongation at break at the higher strain rate indicates that the tensile force could be applied more uniformly to both crystalline β-sheet and amorphous region of dragline silk fibers[3,10]. As a result, the toughness exhibited a 3.0-fold increase as the strain rate increased from 3.3×10^{-5} to 3.3 s^{−1}. The increase in toughness was in agreement with the previous study that found a threefold increase in toughness when varying the strain rate from 1×10^{-3} to 1.7×10^{3} s^{−1} [10].

Scanning electron microscopy observations of fracture surfaces. The fracture surfaces of the dragline silk fibers after tensile tests at RH43% were observed via SEM (Fig. 3). The fracture surfaces of the dragline silk fibers were relatively smooth in the case of strain rates ranging from 3.3×10^{-5} to 3.3×10^{-3} s^{−1}. Meanwhile, the dragline silks showed relatively rough fracture surface when the strain rates more than 3.3×10^{-2} s^{−1} were applied. The dragline silk consists of a hierarchically arranged protein core surrounded by outer skin layers[25]. The protein core is composed of fibrils that are formed by compact assembly of
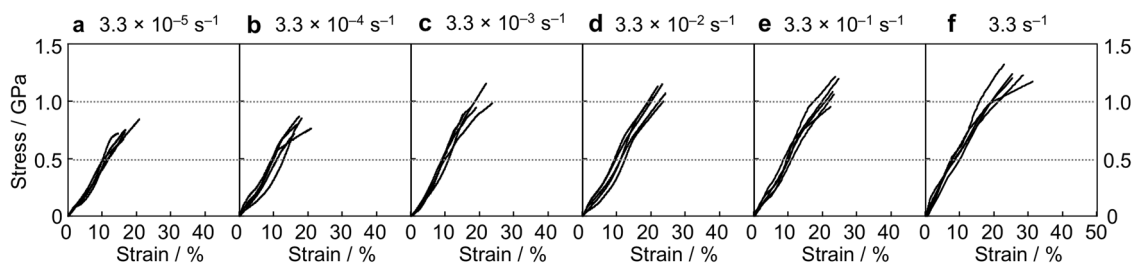
Fig. 1 Effects of strain rates on stress-strain curves of spider dragline silk fibers. Stress–strain curves of spider dragline silk fibers at RH43% under different strain rates: **a** 3.3×10^{-5} s^{−1}, **b** 3.3×10^{-4} s^{−1}, **c** 3.3×10^{-3} s^{−1}, **d** 3.3×10^{-2} s^{−1}, **e** 3.3×10^{-1} s^{−1}, and **f** 3.3 s^{−1}.
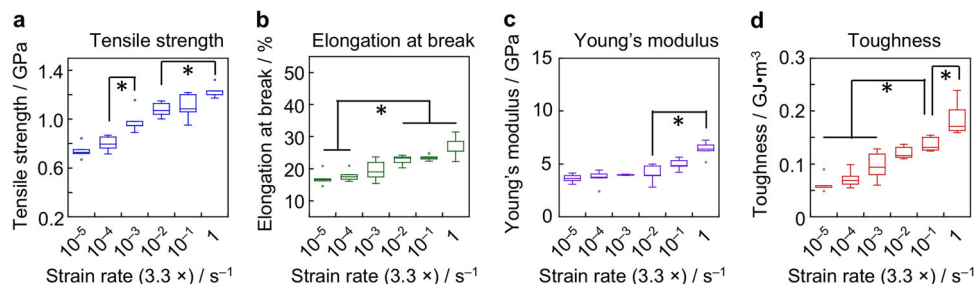
Fig. 2 Effects of strain rates on mechanical properties of spider dragline silk fibers. Mechanical properties of dragline silk fibers at RH43% under strain rates ranging from 3.3×10^{-5} to $3.3\,s^{-1}$: **a** Tensile strength, **b** elongation at break, **c** Young's modulus, and **d** toughness. *Significant differences between groups at $p < 0.05$.
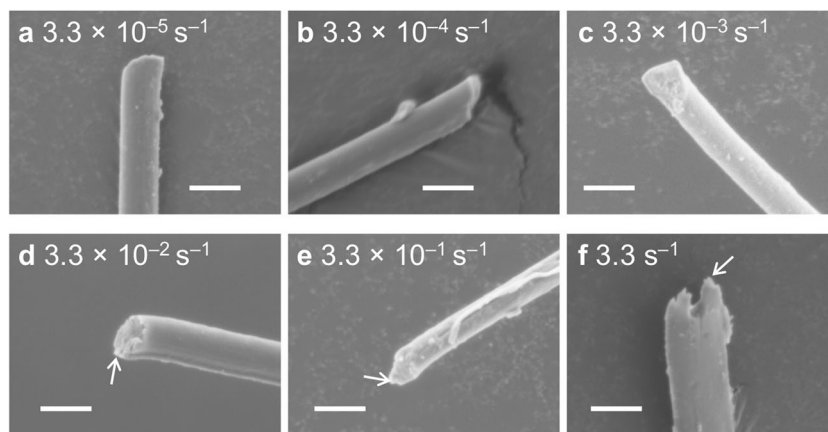

Fig. 3 Effects of strain rates on fracture surfaces of spider dragline silk fibers. SEM images showing the fracture surfaces of the dragline silk fibers at RH43% under different strain rates: **a** $3.3 \times 10^{-5}\,s^{-1}$, **b** $3.3 \times 10^{-4}\,s^{-1}$, **c** $3.3 \times 10^{-3}\,s^{-1}$, **d** $3.3 \times 10^{-2}\,s^{-1}$, **e** $3.3 \times 10^{-1}\,s^{-1}$, and **f** $3.3\,s^{-1}$. Each scale bar denotes $5\,\mu m$. Arrows in (**d**) to (**f**) represent the broken fibrils in the fracture surface.

microfibrils with diameters ranging from 40 to 80 nm[26,27]. The microfibrils form one hierarchical level and could break when the dragline silk fiber is destroyed. Accordingly, a reasonable explanation of the difference in the fracture surface is that the dragline silk fibers could break at macroscopic structural defects as well as at microfibrils at the slower strain rates, while break at microfibrils at the faster strain rates.

Water content of dragline silk fibers incubated under different relative humidity. To prepare dragline silk fibers with various water contents, we used saturated inorganic salt aqueous solutions to set the determined RH according to a previously reported method[28]. The water content in the dragline silk fibers was evaluated with thermogravimetric analysis (TGA), which was performed at 20 °C/min from 30 to 500 °C (Supplementary Fig. 1a). The water content increased in proportion to the RH conditions for the sample preparation. The water content of the dragline silk fiber was 0.5% when the dragline silk fiber was incubated at RH0% (Supplementary Fig. 1b). The water content was determined to be 7.0, 9.3, and 21.2% when the dragline silk fiber was incubated at RH43%, RH75%, and RH97%, respectively (Supplementary Fig. 1b). The thermal degradation of the dragline silk fiber at different RHs was evaluated in terms of a 1%, 5%, and 10% weight decrease (Supplementary Fig. 1c). The degradation temperature of the silk fibers was not related to the humidity levels, implying that the chemical structure of silk was not changed by humidity.

Wide-angle X-ray scattering measurements under different relative humidity. The WAXS measurement of dragline silk fibers was performed at RHs of 0, 43, 75, and 97%. The resultant two-dimensional profiles are displayed in Fig. 4a. A circular smearing of the scattering pattern was detected in the WAXS measurement at RH97% (Fig. 4a–iv). The two-dimensional profiles were converted to one-dimensional profiles through a radial integration of the WAXS data (Fig. 4b). The *d*-spacing values of each plane remained constant upon changing the RHs based on the one-dimensional WAXS profiles, indicating that the crystalline β-sheet structure was not changed by the RH conditions, consistent with the TGA results. The two-dimensional WAXS pattern varied depending on the experimental RH conditions, leading to observable changes in the one-dimensional radial integration profiles, namely, the (211) peak became more conspicuous under higher RH conditions. In addition, the azimuthal intensity profiles of the radially integrated (210) peak are plotted in Fig. 4c. As the RH increased, the full width at half maximum (FWHM) value increased, suggesting a decrease in the orientation of crystalline β-sheets. To estimate the degree of crystallinity, which was calculated from the area of crystalline peaks divided by the total area of crystalline peaks and the amorphous halo, the one-dimensional radial integration profiles were deconvoluted to multiple peaks assigned to the crystalline β-sheets and amorphous halo (Supplementary Fig. 2). The degree of crystallinity was calculated to be constant at ~22% under all RH values investigated. In contrast, we observed changes in FWHM values as a function of RH (Fig. 4d). The FWHM value was 37.5° at RH97% and decreased to 14.5° at RH0%, suggesting that the degree of orientation was higher under lower RH conditions. The crystallite size was calculated by Scherrer's equation using the FWHM of the (210) peak (Fig. 4d), with estimated values of 3.73, 3.74, 3.73, and
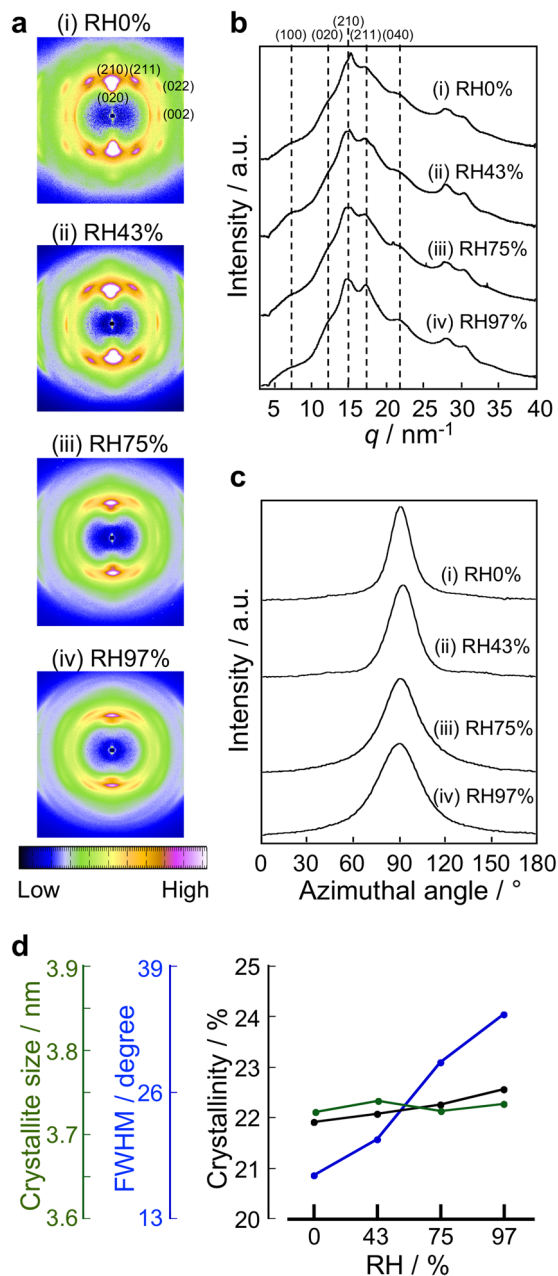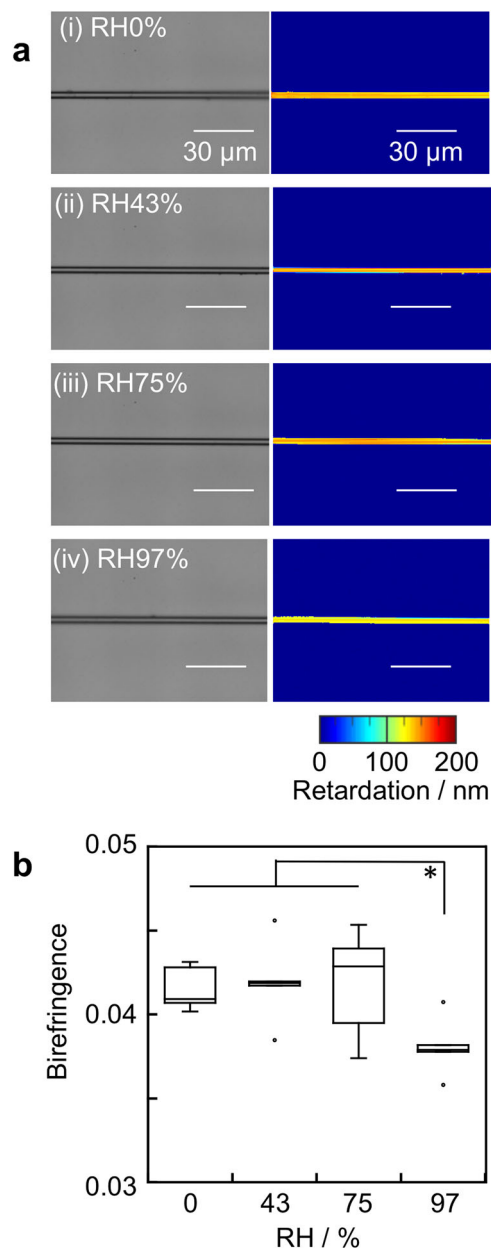
Fig. 4 WAXS measurements of spider dragline silk fibers under different RHs. a Two-dimensional profiles, **b** one-dimensional radial integration profiles, **c** azimuthal intensity profiles of the radially integrated (210) peak, and **d** crystallite size, FWHM, and crystallinity of dragline silk fibers incubated at RHs of (i) 0%, (ii) 43%, (iii) 75%, and (iv) 97%.

Fig. 5 Retardation and birefringence of spider dragline silk fibers. a Optical micrographs and retardation color mapping of spider dragline silk fibers incubated at (i) RH0%, (ii) RH43%, (iii) RH75%, and (iv) RH97%. Each scale bar denotes 30 μm. The retardation values ranged from 0 to 200 nm, as shown in the color scale. **b** Birefringence value as a function of RH. *Significant differences between groups at $p < 0.05$.

3.74 nm at RHs of 0%, 43%, 75%, and 97%, respectively. Thus, crystallite sizes were constant and close to those identified in a previous report[21]. As a result, the high RH condition reduced the degree of orientation of the crystalline β-sheets but did not affect the other crystalline state.

Birefringence measurements under different relative humidity. To evaluate the amorphous region in addition to the crystalline β-sheets, we used birefringence measurements in accordance with our previous study[29]. The retardance values of dragline silk fibers under different RHs was measured, from which the birefringence values were calculated in combination with fiber diameter measurements, obtained via SEM (Fig. 5a). The birefringence values

were found to be approximately constant at around 41.5×10^{-3} between RH0% and RH75% (Fig. 5b). In contrast, a relatively large decrease in birefringence was observed at RH97%, calculated to be $38.0 \times 10^{-3} \pm 1.5 \times 10^{-3}$ (Fig. 5b). The decrease in birefringence at RH97% suggests a more random molecular arrangement of the constituent protein chains, and agrees with the WAXS results presented in Fig. 4d. Water molecules are known to function as plasticizers and induce reorientation of silk molecules in the amorphous region, as observed in the supercontraction of the dragline silk fibers[12,16,30].

Tensile tests under different strain rates and relative humidity. Tensile tests of the dragline silk fibers were conducted at different

strain rates and RHs. The strain rates ranged from 3.3×10^{-5} to $3.3\,s^{-1}$ at RHs of 0, 75, and 97%. The resultant stress–strain curves are displayed in Fig. 6 and Supplementary Fig. 3. The tensile strength and elongation at break tended to increase with increasing strain rate. Mechanical properties at different strain rates and RH conditions were determined from the stress–strain curves (Fig. 7). The tensile strength, elongation at break, and Young's modulus increased linearly as the strain rate increased, regardless of the experimental RH conditions. The tensile

strength increased approximately 1.4-, 2.3-, and 1.5-fold as the strain rate increased from 3.3×10^{-5} to $3.3\,s^{-1}$ at RH0%, RH43%, and RH97%, respectively. The effect of RHs on the mechanical properties was characterized (Supplementary Figs. 4–7). The tensile strength decreased as the RH increased (Supplementary Fig. 4), which is similar to the trend reported in a previous study[5]. The elongation at break increased as the RH increased under all the strain rates utilized in this study (Supplementary Fig. 5). Regardless of the applied strain rates, the elongation at break at
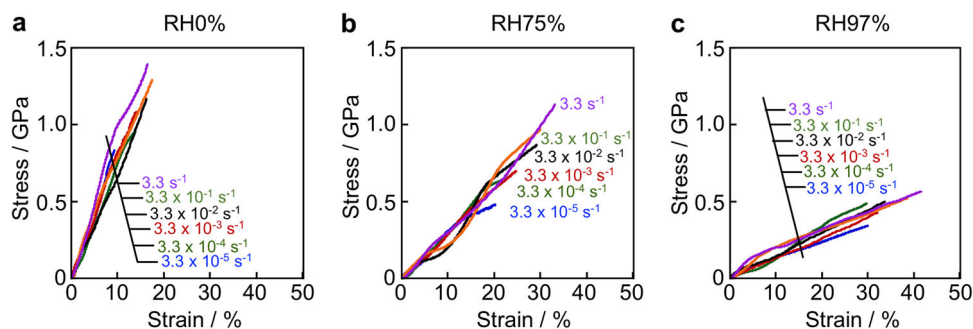
Fig. 6 Humidity effects on stress-strain curves of spider dragline silk fibers. Stress–strain curves of spider dragline silk fibers at **a** RH0%, **b** RH75%, and **c** RH97% under different strain rates ranging from 3.3×10^{-5} to $3.3\,s^{-1}$.
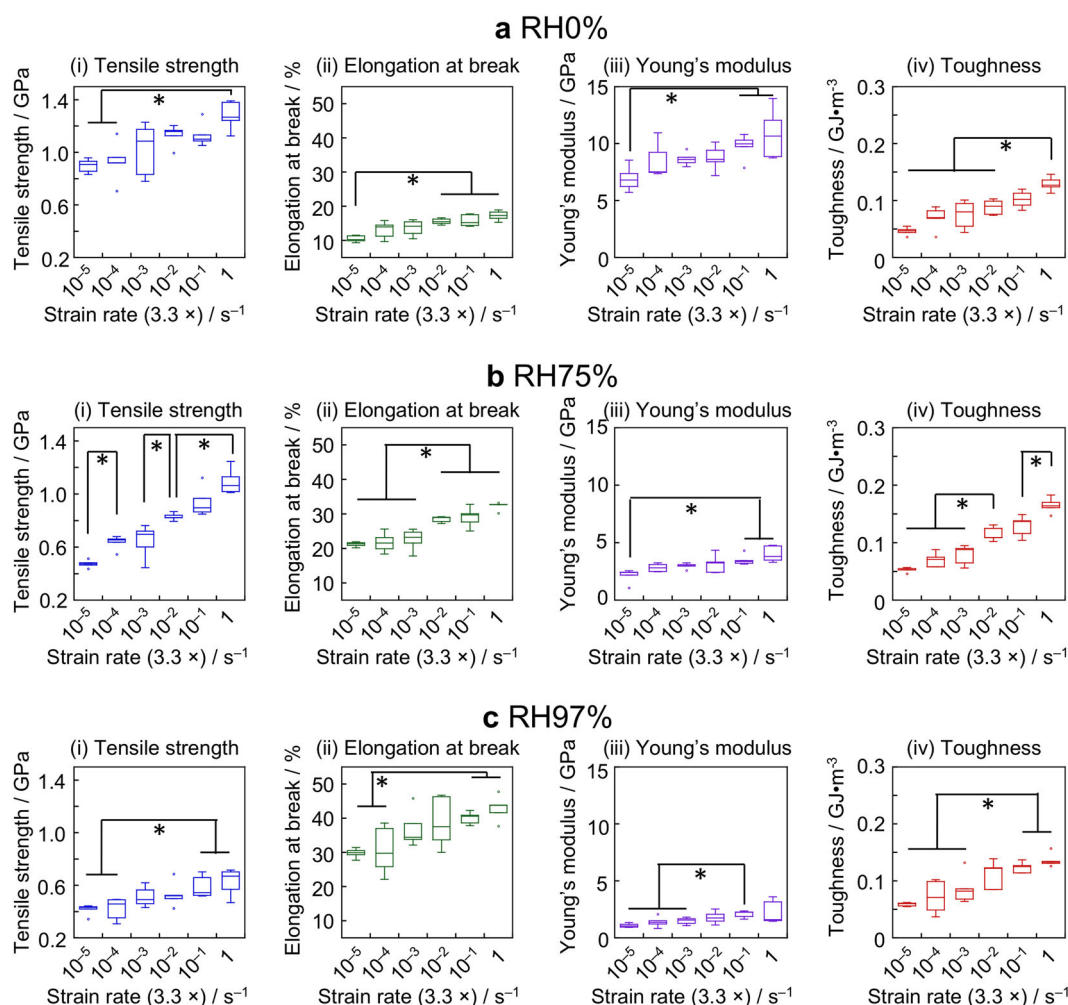
Fig. 7 Humidity effects on mechanical properties of spider dragline silk fibers. Mechanical properties of dragline silk fibers at **a** RH0%, **b** RH75%, and **c** RH97% under strain rates ranging from 3.3×10^{-5} to $3.3\,s^{-1}$: (i) tensile strength, (ii) elongation at break, (iii) Young's modulus, and (iv) toughness. *Significant differences between groups at $p < 0.05$.

RH97% was approximately twofold higher than that at RH0%. The Young's modulus linearly decreased as the RH increased (Supplementary Fig. 6). As discussed in the previous paragraph, the decrease in Young's modulus originated from the plasticization effect of water molecules at high RH conditions[11,12,14,17,30]. The toughness of the dragline silk was not significantly changed by the RH conditions at strain rates ranging from 3.3×10^{-5} to 3.3×10^{-1} s^{-1} (Supplementary Fig. 7). In contrast, at a strain rate of 3.3 s^{-1}, the toughness was highest at RH43%, followed by the toughness at RH75%. Overall, at RH0%, the toughness at high deformation rates originated from the increase in yield stress, whereas the dragline at RH75% and RH97% exhibited rubber-like behavior because of the increase in rubbery components induced by water plasticization.

Dragline silk fibers are used by spiders as a lifeline to prevent unexpected falling and to capture prey, such as flying insects. Strain rates >1 s^{-1} are thought to be applied to the dragline silk fibers in the natural state[3]. This natural range of strain rates is in agreement with the range of strain rates selected in this study, wherein the toughness of the dragline silk at RH43% and RH75% was higher than that at RH0% and RH97%. The environmental humidity in the natural habitat of spiders could be moderate. Based on the effect of RH on toughness at a strain rate of 3.3 s^{-1}, the spider dragline silk fibers might evolve to exhibit toughness at a moderate RH, namely, a naturally humid environment and the relatively high deformation rates that occur in natural spider behaviors.

The fracture surfaces of the dragline silks after tensile testing at RHs of 0, 75, and 97% were observed via SEM (Supplementary Fig. 8). The fracture surfaces of the dragline tended to be smooth at relatively low strain rates ranging from 3.3×10^{-5} to 3.3×10^{-2} s^{-1}, whereas the fracture surfaces were rough under relatively high strain rates ranging from 3.3×10^{-1} to 3.3 s^{-1}, as was the case with RH43%. Thus, the dragline silk was broken at the microfibril level at faster deformation, regardless of the humidity conditions.

Simultaneous wide-angle X-ray scattering-tensile test measurements. To investigate the structural changes upon extension at different RH conditions, we performed WAXS and tensile tests simultaneously using the experimental setup shown in Supplementary Fig. 9a, b. This experimental setup could not use a single dragline silk fiber; a bundle of the fibers was needed to gain sufficient scattering intensity in the WAXS measurements (Supplementary Fig. 9c). The bundle of dragline silk fibers consisted of ~400–600 dragline fibers. Two supplemental jigs were attached in the tensile test devices to prevent vibration of the fiber bundle (Supplementary Fig. 9d). The stress–strain curves and the corresponding two-dimensional WAXS data at RH43% and the other humidity conditions are shown in Fig. 8 and Supplementary Figs. 10–12, respectively. Because the diameter of the dragline silk bundle could not be measured precisely, an arbitrary unit was applied as the unit of stress in the stress–strain curves, where the maximum tensile strength was set at 100. The X-ray beam was radiated at 12 intervals upon extension deformation, as shown in the stress–strain curves. In the simultaneous WAXS-tensile tests, the X-ray beam was radiated continuously on the sample at certain intervals upon extension. Considering these settings mentioned above, we successfully monitored the WAXS profiles during stretching deformation.
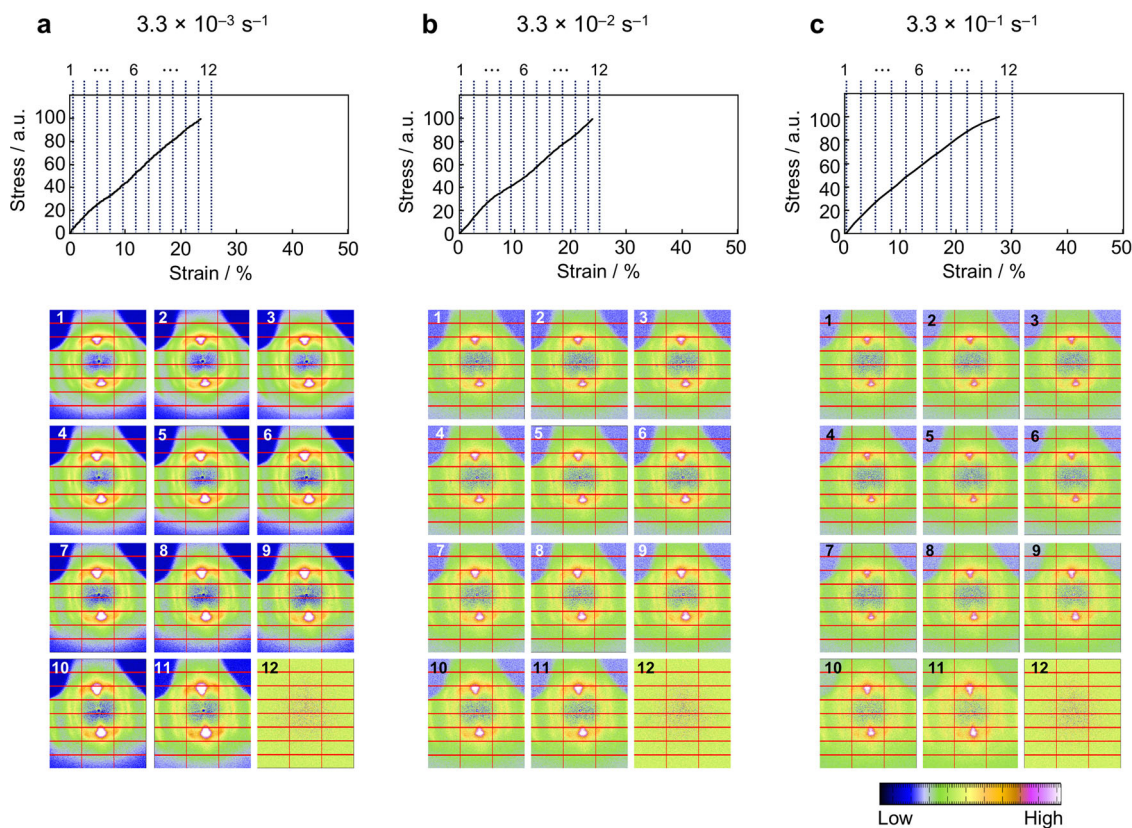
Fig. 8 Structural analysis of spider draglien upon extension. Two-dimensional WAXS profiles at strain rates of **a** 3.3×10^{-3} s^{-1}, **b** 3.3×10^{-2} s^{-1}, and **c** 3.3×10^{-1} s^{-1} using spider dragline silk fibers at RH43%. The simultaneous WAXS-tensile tests prevented us from making a composite image from the resultant WAXS data. Thus, the boundary of each camera detector remained in the overall scattering images because the single detector could not detect all the scattering of whole sample areas. The boundary of the camera detector is masked, which is highlighted by red lines.
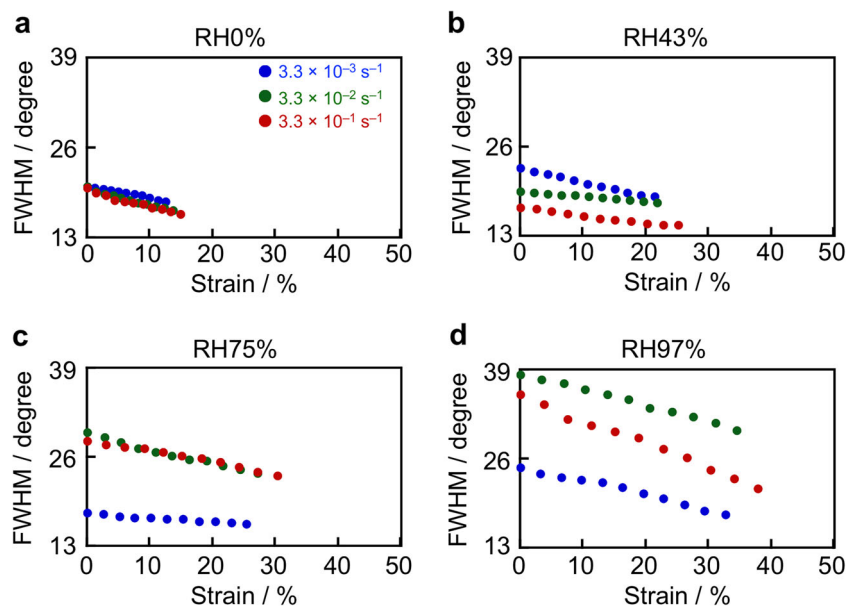
Fig. 9 FWHM of the spider dragline silk fiber as a function of strain under different strain rates. FWHM calculated from the azimuthal intensity WAXS profiles of the radially integrated (210) peak in the simultaneous WAXS-tensile test under different RHs: **a** RH0%, **b** RH43%, **c** RH75%, and **d** RH97%. The blue, green, and red dots denote strain rates of $3.3 \times 10^{-3}\,s^{-1}$, $3.3 \times 10^{-2}\,s^{-1}$, and $3.3 \times 10^{-1}\,s^{-1}$, respectively.

To evaluate the changes in the FWHM value upon extension, the two-dimensional WAXS data were converted to azimuthal intensity profiles of the radially integrated (210) peak at different RHs (Supplementary Figs. 13–16). The FWHM values as a function of strain at different RHs are plotted in Fig. 9. Under all four RH conditions used in this study, the FWHM value decreased as the strain increased. At the initial state (zero strain), the FWHM values were higher at higher RHs, indicating that the orientation of the crystalline β-sheets of the silk fiber was aligned more randomly at higher RH conditions. Based on the FWHM values obtained in the simultaneous WAXS-tensile test, the molecular mobility was lower under less humid conditions, which was not sufficient to induce the reorientation of the crystalline β-sheets by stretching deformation.

The two-dimensional WAXS data were also converted to one-dimensional radial integration profiles under different RHs (Supplementary Figs. 17–20). The crystallite sizes as a function of strain were calculated from the FWHM of (210) peaks of the one-dimensional profiles (Supplementary Fig. 21). The (210) peak corresponds to the direction along the hydrogen bonds of the crystalline β-sheets and is denoted here as the *b*-axis of the crystallite[31]. The crystallite sizes were slightly decreased upon extension, regardless of the RHs and strain rates. Because the mobility of silk molecular chains could be enhanced by a plasticization effect of water molecules at high RH condition, it would be expected that the amorphous entropy elastic stretching preferentially happens, instead of unfolding and breaking at the crystalline region. However, our results demonstrate that the crystallite size decreased even at low deformation range at high RH. Glišović et al. also reported the crystallite size decrease upon stretching using the *Nephila* dragline silk which was immersed in water[20]. The decrease in crystallite size can be originated from a partial splitting of the crystallites along the noncovalent bonds or an unfolding of silk chains at the interface of the amorphous region[20]. Glišović et al. calculated the total energy, which is necessary to break the hydrogen bonds, in the crystallite and compared with the typical stretching energy needed in the tensile tests. The result indicates that the total energy which is necessary to break the hydrogen bonds is in the same range as the total

energy for stretching in the tensile test data[20]. The crystallinity did not change significantly under the measured RHs and strain rates (Supplementary Fig. 22). Thus, crystal regions tend to be deformed upon extension at low RH, and both crystalline and amorphous regions are thought to be deformed upon extension at high RH. This phenomenon occurs because when the amorphous motility is high, the silk behaves as a rubber-like elastomer and molecular reorientation easily occurs. On the other hand, in the dry state, the silk behaves like a plastic material, and the efficiency of reorientation is lower. In the natural condition for Japanese *Nephila* spiders, namely, at moderate humidity, the spider dragline is a rubber-like elastomer with high strength originating from oriented crystalline β-sheets.

Madurga et al. have devised an alignment parameter to correlate between molecular alignment and mechanical performances of dragline silks of spiders across the broad phylogeny[32]. Comparisons of such an alignment parameter across different humidity and strain rates would enable for a more comprehensive examination of the data. However, the mechanical properties of dragline silks in the present study are influenced not only by molecular alignment but also by humidity owing to the plasticizing effect of water molecules, unlike the case by Madurga et al. Instead of using alignment parameter, we compared the mechanical properties of dragline silks directly with the applied humidity in Supplementary Figs. 4–7.

In the present study, we investigated the effect of strain rates on the mechanical and structural properties of spider dragline silk fibers under different RH conditions. The tensile strength improved as the strain rate increased. Although the increase in tensile strength with increasing strain rate was smaller at RH97%, the high elongation at break at RH97% contributed to maintaining the toughness value of the dragline silk fibers. The fracture surfaces of the dragline fibers were observed via SEM, demonstrating that the fracture surfaces were relatively smooth at lower deformation rates and rough at higher deformation rates. The resultant fracture surfaces indicated that the dragline silk fibers were broken at macroscopic structural defects at lower deformation rates, whereas the fibers were broken at microfibrils at higher deformation rates. Water molecules could be substituted
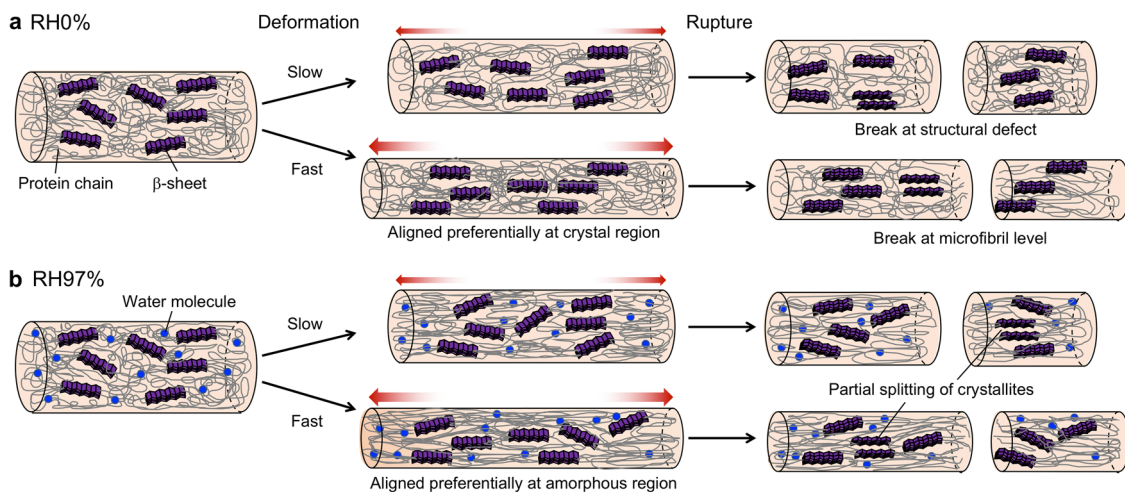
Fig. 10 A schematic model demonstrating microstructural changes of spider dragline silk fibers at different strain rates and humidity. Silk molecular chains at crystal region deform and align along the fiber axis at dry condition, whereas water molecules bind to amorphous regions and facilitate the molecular movement at wet condition. With further stretching, the crystallites start to split. The fracture surfaces would be detected at the structural defect at slower deformation rate, while the dragline silk could be broken at the microfibril level rather than at a macroscopic structural defect at faster deformation rate.

with the intermolecular hydrogen bonding between silk molecular chains, inducing easy flow under the application of load. At high RH condition, the dragline silk has a highly disordered structure, which was confirmed by the lower birefringence and degree of orientation in the present study. Thus, the creep and stress relaxation behavior of spider dragline silks are expected to be higher at high RH condition and it is speculated that the fracture surfaces would be detected at the structural defect under higher RH condition. However, the SEM observation of the fracture surface after the tensile test demonstrated that the fracture surfaces of the dragline silks tended to be smooth at relatively low strain rates, whereas the fracture surfaces were rough under relatively high strain rates, regardless of the experimental RH. The rough fracture surfaces of the dragline silk fibers suggest that the fibers were broken at the microfibril level at faster deformation rate. Even though the mobility of silk molecular chain is facilitated under high RH condition, the tensile force was applied to both crystal and amorphous region, which was confirmed by the crystallite size decrease based on the simultaneous WAXS-tensile test. Hence, the load is expected to be applied to the microfibrils of spider dragline silks during stretching at higher deformation rate before the stress relaxation completed. Accordingly, the dragline silk could be broken at the microfibril level rather than at a macroscopic structural defect at faster deformation rate. Combined with the SEM observation and simultaneous WAXS-tensile test, microstructural changes of spider dragline silk fibers could be depicted in Fig. 10.

The individual technique applied in this study was already used to determine the humidity- and stain rate-dependent structural changes of the dragline silk as well as mechanical properties. However, as far as we know, no study has been performed to change the humidity- and strain rate simultaneously. The dragline silk fibers exhibited the same degree of toughness at strain rates ranging from 3.3×10^{-5} to $3.3 \times 10^{-1}\,\mathrm{s}^{-1}$, regardless of the experimental humidity. The toughness was enhanced at moderate RH in the case of the highest strain rate of $3.3\,\mathrm{s}^{-1}$, which is similar to that occurring in nature. The structural changes upon extension deformation were monitored with a simultaneous WAXS-tensile test. There was no observable change in crystallinity during stretching, whereas the crystallite size decreased, and the degree of orientation increased in the process of extension deformation. Thus, we conclude that the *Nephila*

clavata dragline silk is optimized to exert its toughness at relatively high deformation rates and at moderate RHs in the natural condition for Japanese *Nephila* spiders, especially *Nephila clavata*. Simulations using multibody dynamic model have demonstrated that the extremely high or low humidity has negative effects on web capture ability of spiders, which is improved with the data presented herein. Further studies investigating the time for creep and stress relaxation behavior at different humidity should be needed to elucidate the interplay between strain rates and mechanical responses. These findings will help to understand the natural design of spider dragline silk fibers exhibiting excellent strength and ductility upon deformation and will contribute to realizing artificial spider silk-like structural materials.

Methods

Collection of spider dragline silk fibers. The spider dragline silk fibers were collected from *Nephila clavata* females at ~21 mm/s. The spider silk fibers were kept in lightproof boxes at RHs ranging from 30 to 50% to prevent the fibers from ultraviolet (UV) damage and drying.

Preparation of dragline silk fibers with different water contents. The dragline silk fibers were incubated at 25 °C for 48 h under various RHs, which was controlled by silica gel for RH0% or by saturated water vapor of inorganic salts for the other RHs, in accordance with a previously reported method[28]. The inorganic salts used in this study were potassium carbonate (RH43%), sodium chloride (RH75%), and potassium sulfate (RH97%). Then, the dragline silk fibers incubated under different RHs were fixed to the sample holder with cyanoacrylate adhesive for tensile testing and were incubated under the corresponding RH condition until the tensile test was performed.

Tensile tests. Tensile tests of the single dragline silk fibers were conducted with a mechanical testing apparatus (EZ-LX/TRAPEZIUM X, Shimadzu, Kyoto, Japan) equipped with a sealed chamber and humidity generator (Kitz Microfilter, Nagano, Japan). The initial length of the single dragline silk fiber was set to 5 mm. The extension speed was applied ranging from 0.01 to 1000 mm/min, and the force during testing was measured with a 1 N load cell. The tensile strength, Young's modulus, elongation at break, and toughness were obtained from the resultant stress–strain curves. Statistical analysis was conducted with a Student's *t*-test.

Scanning electron microscopy observations. The surface morphology and cross section of the dragline silk fibers were assessed via SEM (JCM 6000, JEOL Ltd., Tokyo, Japan). The samples were mounted on an aluminum stub with conductive tape and sputter-coated with gold for 1 min with a Smart Coater (JEOL, Tokyo, Japan) prior to SEM visualization at 5 kV.

Wide-angle X-ray scattering measurement. Synchrotron WAXS measurements were conducted at the BL45XU beamline of SPring-8, Harima, Japan, in accordance with a previous report[28]. The X-ray energy was 12.4 keV at a wavelength of 0.1 nm, the sample-to-detector distance for the WAXS measurements was 255 mm, and the exposure time for each diffraction pattern was 10 s. The measurement was performed three times for each sample, and the resultant three two-dimensional WAXS images were composited. A beam with a diameter of 45 μm was applied. All WAXS patterns were recorded with a flat panel detector (FPD, C9728DK-10, Hamamatsu Photonics, Japan). The measurements were performed under a controlled RH. The resultant two-dimensional WAXS data were converted into one-dimensional profiles with the software Fit2D[33]. The data were corrected for background scattering, and the crystallinity was calculated from the area of crystal peaks divided by the total area of crystal peaks and the amorphous halo by fitting the Gaussian function with Igor Pro 6.3 (WaveMetrics, Inc., Portland, OR).

The crystallite sizes, determined from the (210) diffraction peak, were evaluated by Scherrer's equation, as shown in Eq. (1):

$$D = \frac{K\lambda}{\beta \cos\theta} \tag{1}$$

where D is the crystallite size, K is the shape factor, λ is the wavelength of the X-ray beam, β is the FWHM of the scattering peak and θ is the corresponding Bragg angle. We used a value of 0.9 for the shape factor based on a previous report[20].

Birefringence measurement. The retardation provided by the silk fiber was measured with a birefringence measurement system WPA-100 (Photonic Lattice Inc., Miyagi, Japan) and was analyzed with WPA-VIEW (version 1.05) software, in accordance with a previous method[29]. The birefringence of the dragline silk fiber was calculated from the retardation and silk fiber diameter, which was determined via SEM.

Thermogravimetric analysis. The (thermogravimetric analysis) TGA of the dragline silk was conducted with a TGA/DSC2 (Mettler Toledo, Greifensee, Switzerland) in accordance with a previous method[28]. The dragline silk (1 mg) was weighed in an aluminum pan and then heated at 20 °C/min from 30 to 500 °C under a nitrogen atmosphere. The lid of the aluminum pan had a pinhole for allowing water flow to prevent the pan from bursting due to an increase in the internal pressure during the heating process. The device was calibrated with an empty pan to form a baseline and calibrated with indium to characterize the heat flow and temperature of the system. The water content of each dragline silk fiber was calculated as the total amount of water obtained from the TGA data divided by the total weight of the dragline silk fibers.

Simultaneous wide-angle X-ray scattering-tensile test. A sample stretching apparatus (Sentech, Osaka, Japan) was placed in the experimental hutch and controlled outside of the hutch at the BL45XU beamline of SPring-8. The dragline silk fibers were attached to the stretching apparatus. The initial length of the fiber bundle between the fixtures was 13 mm. Three kinds of strain rates were applied to the fibers: 3.3×10^{-3}, 3.3×10^{-2}, and 3.3×10^{-1} s^{-1}. The exposure time for each scattering pattern was 1, 0.4, and 0.099 s for the strain rates of 3.3×10^{-3}, 3.3×10^{-2}, and 3.3×10^{-1} s^{-1}, respectively. The measurements were performed at 25 °C under the determined RH, which was controlled with a humidity generator (Sensirion, Tokyo, Japan). The intensities and FWHM values of all the peaks were estimated by fitting Gaussian profiles with Igor Pro 6.3.

Data availability

All data supporting the findings of this study are available within the article, as well as the Supplementary Information file, or available from the corresponding author on reasonable request.

References

1. Cranford, S. W., Tarakanova, A., Pugno, N. M. & Buehler, M. J. Nonlinear material behaviour of spider silk yields robust webs. *Nature* **482**, 72–76 (2012).
2. Holland, C., Numata, K., Rnjak-Kovacina, J. & Seib, F. P. The biomedical use of silk: past, present, future. *Adv. Health. Mater.* **8**, 1800465 (2019).
3. Gosline, J. M., Guerette, P. A., Ortlepp, C. S. & Savage, K. N. The mechanical design of spider silks: from fibroin sequence to mechanical function. *J. Exp. Biol.* **202**, 3295–3303 (1999).
4. Blamires, S. J. & Sellers, W. I. Modelling temperature and humidity effects on web performance: implications for predicting orb-web spider (*Argiope* spp.) foraging under Australian climate change scenarios. *Conserv. Physiol.* **7**, coz083 (2019).
5. Vehoff, T., Glisovic, A., Schollmeyer, H., Zippelius, A. & Salditt, T. Mechanical properties of spider dragline silk: humidity, hysteresis, and relaxation. *Biophys. J.* **93**, 4425–4432 (2007).
6. Blamires, S. J. et al. Mechanical performance of spider silk is robust to nutrient-mediated changes in protein composition. *Biomacromolecules* **16**, 1218–1225 (2015).
7. Nie, X., Song, B., Ge, Y., Chen, W. W. & Weerasooriya, T. Dynamic tensile testing of soft materials. *Exp. Mech.* **49**, 451–458 (2008).
8. Cunniff, P. M. et al. Mechanical and thermal properties of dragline silk from the spider Nephila clavipes. *Polym. Adv. Technol.* **5**, 401–410 (1994).
9. Denny, M. The physical properties of spider's silk and their role in the design of orb-webs. *J. Exp. Biol.* **65**, 483–506 (1976).
10. Hudspeth, M., Nie, X., Chen, W. & Lewis, R. Effect of loading rate on mechanical properties and fracture morphology of spider silk. *Biomacromolecules* **13**, 2240–2246 (2012).
11. Blackledge, T. A. et al. How super is supercontraction? Persistent versus cyclic responses to humidity in spider dragline silk. *J. Exp. Biol.* **212**, 1981–1989 (2009).
12. Boutry, C. & Blackledge, T. A. Wet webs work better: humidity, supercontraction and the performance of spider orb webs. *J. Exp. Biol.* **216**, 3606–3610 (2013).
13. Brown, C. P. et al. The critical role of water in spider silk and its consequence for protein mechanics. *Nanoscale* **3**, 3805–3811 (2011).
14. Elices, M., Plaza, G. R., Perez-Riguiero, J. & Guinea, G. V. The hidden link between supercontraction and mechanical behavior of spider silks. *J. Mech. Behav. Biomed. Mater.* **4**, 658–669 (2011).
15. Fu, C., Porter, D. & Shao, Z. Moisture effects on *Antheraea pernyi* silk's mechanical property. *Macromolecules* **42**, 7877–7880 (2009).
16. Giesa, T., Schuetz, R., Fratzl, P., Buehler, M. J. & Masic, A. Unraveling the molecular requirements for macroscopic silk supercontraction. *ACS Nano* **11**, 9750–9758 (2017).
17. Liu, Y., Shao, Z. & Vollrath, F. Relationships between supercontraction and mechanical properties of spider silk. *Nat. Mater.* **4**, 901 (2005).
18. Opell, B. D., Buccella, K. E., Godwin, M. K., Rivas, M. X. & Hendricks, M. L. Humidity-mediated changes in an orb spider's glycoprotein adhesive impact prey retention time. *J. Exp. Biol.* **220**, 1313–1321 (2017).
19. Vollrath, F. & Edmonds, D. T. Modulation of the mechanical properties of spider silk by coating with water. *Nature* **340**, 305 (1989).
20. Glišović, A., Vehoff, T., Davies, R. J. & Salditt, T. Strain dependent structural changes of spider dragline silk. *Macromolecules* **41**, 390–398 (2008).
21. Grubb, D. T. & Jelinski, L. W. Fiber morphology of spider silk: the effects of tensile deformation. *Macromolecules* **30**, 2860–2867 (1997).
22. Numata, K. et al. Use of extension-deformation-based crystallisation of silk fibres to differentiate their functions in nature. *Soft Matter* **11**, 6335–6342 (2015).
23. Sirichaisit, J., Brookes, V. L., Young, R. J. & Vollrath, F. Analysis of structure/property relationships in silkworm (*Bombyx mori*) and spider dragline (*Nephila edulis*) silks using Raman spectroscopy. *Biomacromolecules* **4**, 387–394 (2003).
24. Sirichaisit, J., Young, R. J. & Vollrath, F. Molecular deformation in spider dragline silk subjected to stress. *Polymer* **41**, 1223–1227 (2000).
25. Yazawa, K., Malay, A. D., Masunaga, H. & Numata, K. Role of skin layers on mechanical properties and supercontraction of spider dragline silk fiber. *Macromol. Biosci.* **19**, e1800220 (2019).
26. Du, N. et al. Design of superior spider silk: from nanostructure to mechanical properties. *Biophys. J.* **91**, 4528–4535 (2006).
27. Lin, T.-Y. et al. Liquid crystalline granules align in a hierarchical structure to produce spider dragline microfibrils. *Biomacromolecules* **18**, 1350–1355 (2017).
28. Yazawa, K., Ishida, K., Masunaga, H., Hikima, T. & Numata, K. Influence of water content on the β-sheet formation, thermal stability, water removal, and mechanical properties of silk materials. *Biomacromolecules* **17**, 1057–1066 (2016).
29. Numata, K., Sato, R., Yazawa, K., Hikima, T. & Masunaga, H. Crystal structure and physical properties of *Antheraea yamamai* silk fibers: long poly(alanine) sequences are partially in the crystalline region. *Polymer* **77**, 87–94 (2015).
30. Guinea, G. V., Elices, M., Perez-Riguiero, J. & Plaza, G. R. Stretching of supercontracted fibers: a link between spinning and the variability of spider silk. *J. Exp. Biol.* **208**, 25–30 (2005).
31. Sampath, S. et al. X-ray diffraction study of nanocrystalline and amorphous structure within major and minor ampullate dragline spider silks. *Soft Matter* **8**, 6713–6722 (2012).
32. Madurga, R. et al. Material properties of evolutionary diverse spider silks described by variation in a single structural parameter. *Sci. Rep.* **6**, 18991 (2016).
33. Hammersley, A. P., Svensson, S. O., Hanfland, M., Fitch, A. N. & Hausermann, D. Two-dimensional detector software: from real detector to idealised image or two-theta scan. *High Press. Res.* **14**, 235–248 (1996).

Author contributions
Y.N.R. and K.N. designed the research. H.M and K.Y. performed the WAXS measurements and characterized the WAXS results. K.Y. and A.D.M. prepared the samples. K.Y. and K.N. analyzed the whole data in the context of the physical properties of the dragline. All the authors prepared the paper.

Competing interests
The authors declare no competing interests.

Additional information
Supplementary information is available for this paper at https://doi.org/10.1038/s43246-020-0011-8.

Correspondence and requests for materials should be addressed to K.N.

Reprints and permission information is available at http://www.nature.com/reprints

Publisher's note Springer Nature remains neutral with regard to jurisdictional claims in published maps and institutional affiliations.